# SPAD Image Sensors for Quantum and Classical Imaging

**Prof. Dr. Edoardo Charbon**
EPFL
Rue de la Maladière 71b, 2002 Neuchâtel
SWITZERLAND

edoardo.charbon@epfl.ch

## ABSTRACT

*Single-photon avalanche diodes (SPADs) have been demonstrated on a variety of CMOS technologies since the early 2000s. While initially inferior to their counterparts implemented dedicated technologies, modern CMOS SPADs have recently matched them in sensitivity, noise, and timing jitter. Indeed, high time resolution, enabled by low jitter, has helped demonstrate the most impressive developments in fields of imaging and detection, including fluorescence lifetime imaging microscopy (FLIM), Förster resonance energy transfer (FRET), fluorescence correlation spectroscopy (FCS), time-of-flight positron emission tomography (TOF-PET), and light detection and ranging (LiDAR), just to name a few. The SPAD's power of detecting single photons in pixels that can be replicated in great numbers, typically in the millions, is currently having a major impact in computational imaging and quantum imaging. These two emerging disciplines stand to take advantage of larger and larger SPAD image sensors with increasingly low jitter and noise, and high sensitivity. Finally, due to the computational power required at pixel level, power consumption must be reduced; we thus advocate the use of* in situ *computational engines, which, thanks of CMOS' economy of scale and 3D-stacking, enable vast computation density. Some examples of this trend are given, along with a general perspective on SPAD image sensors.*

## 1.0 INTRODUCTION

A single-photon avalanche diode (SPAD) is a reverse-biased photodiode operating above breakdown voltage, a regime generally referred to as Geiger mode of operation [1]. Thus, SPADs are often called Geiger-mode avalanche photodiodes (GM-APDs). Due the high electric fields in play, designed to achieve impact ionization, a conventional planar photodiode needs to be modified, so as to prevent premature edge breakdown.

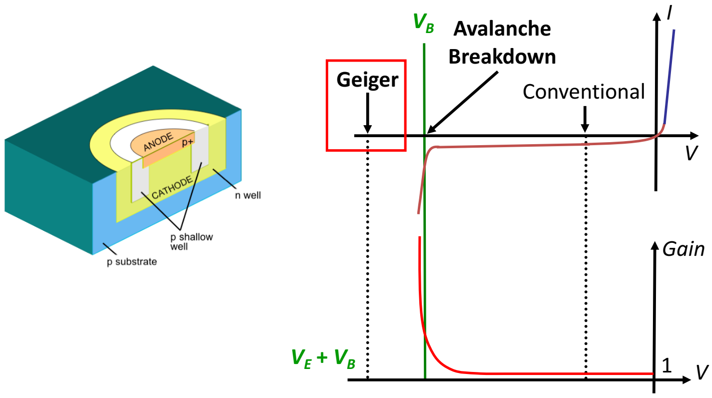


**Figure 198-1: Generic SPAD cross-section and operation.**

The figure above shows the typical cross-section of a SPAD and the biasing regime to achieve Geiger mode of operation, thereby enabling virtually infinite optical gain and thus single-photon detectability. The figure also shows important parameters, such as the breakdown voltage ($V_B$) and excess bias voltage ($V_E$), i.e. the voltage in excess of the breakdown used for biasing the SPAD. To avoid the destruction of SPADs, it is necessary to quench the avalanche as quickly as possible and to recharge the device to its original idle voltage. The figure below describes a possible scheme, known as passive quenching, that can be used for this purpose. Other schemes, involving active quenching and/or recharge, are also known in the literature. It is important to note that fast quenching can have positive implications in the reduction of afterpulsing and timing jitter, but also in long-term reliability of SPADs. Fast recharge mostly reduces dead time, which in turn increases the maximum photon flux one can detect; it can also be used to control afterpulsing probability [2-4].

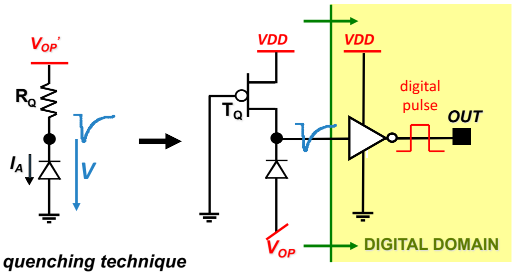


**Figure 198-2: SPAD passive quenching and conversion to a digital signal.**

A CMOS SPAD can achieve today sub-10ps timing resolution, measured as single-photon time resolution (SPTR) [5,46,47], while recently SPADs have reported sensitivity, measured as photon detection probability (PDP), as high as 90% [42]. Photon detection efficiency (PDE) is often reported and it is defined as PDP×FF, where FF denotes the fill factor, i.e. the ratio between active area and total area of the pixel. Another important performance measure for SPADs is dark count rate (DCR), which relates to counts measured in the SPAD in the dark on average [6-8]. With the introduction of CMOS SPADs in 2003 [9], new scalable devices have appeared, with the possibility of integrating thousands or millions on the same chip [10-14]. New performance measures have thus emerged, which relate to large arrays, such as crosstalk both of optical and electrical nature, and the uniformity of performance measures, such as dead time, PDP/PDE, DCR, and SPTR. Uniformity is usually defined in %-variation over the area of the chip, and it is usually a function of technology, temperature, and excess bias voltage.

To achieve large-format SPAD image sensors, it was necessary to scale SPADs down to smaller dimensions, so as to achieve small pitch pixels. This required the development of SPADs in deep-submicron CMOS technologies. Over the years, 180-nm, 160-nm, 150-nm, 130-nm, 110-nm, 65-nm, 55-nm, and 40-nm SPADs were thus created [15-25], whereas SOI SPADs [20], p-i-n SPADs [21], and subsequently backside-illuminated (BSI) SPADs were developed to enable 3D-stacking, which was introduced in 2015 [26]. With 3D-stacking it was now possible to implement complex functionality back-to-back with the SPADs. Moreover, SPAD optimization could now be decoupled from logic and mixed-signal design miniaturization, thus enabling further improvement of density. As a result, a flurry of applications of SPADs appeared in the biomedical [27,28] field, in LiDAR [29], and many other applications requiring time-resolved imaging, including a new emerging field of research: quantum imaging [30].

Thanks to all these advances, in the mid-2010s, researchers began increasing pixel counts [31] to achieve the megapixel milestone in 2020 [32]. 3D-stacking and BSI SPADs advanced as well, with the creation of architectures that could enable higher excess bias and thus higher PDE and better SPTR [33]. Moreover, research on high-dynamic range imaging could yield a better understanding of SPAD operation, especially at low and high illumination regimes [34,35]. New materials are available today for the extension of SPAD PDE, especially in the near infrared spectrum [36], along with more advanced models thanks to a deep understanding of the physics of avalanching [37-41] as well as alternative methods to detect single photons [40]. Even traditional CMOS SPADs have continued to advance and have now become commonplace in consumer electronics [43-47]. The table below summarizes recent achievements in CMOS SPADs in terms of the performance measures described above.

**Table 198-1. Summary of SPAD performance [46].**

| Comparative Table | | | | | | | | | |
|---|---|---|---|---|---|---|---|---|---|
| | Technology (nm) | Diameter $\mu m$ | $V_{EX}/V_{BD}$ (V) | Peak PDP (%) @$\lambda$ (nm) | PDP (%) @850 nm | DCR/unit area ($cps/\mu m^2$) | AP (%) | Jitter (ps) | FoM$_T$ [44] |
| Ghioni [7] | Custom Thin | 50-200 | 5-10/30-35 | 52-68 @550 | 12-15 | 0.4-1.6[a] | 2[b] | 35[c] | 1.88E+11 |
| Gulinatti [8] | Custom RE | 50 | 20/45-55 | 58 @650 | 28 | 0.3[d] | N/A | 93[c] | N/A |
| Villa [16] | 350 | 10-500 | 2-6/25 | 37-53 @450 | 2-4.5 | 0.05[a] | 1[e] | 90[f] | 6.52E+11 |
| Leitner [17] | 180 | 10 | 1-3.3/21 | 35-47 @450 | N/A[g] | 0.3-1.8[a] | N/A | N/A | N/A |
| Veerappan [18] | 180 | 12 | 2-10/23.5 | 24-48 @480 | 3-8 | 0.16-176[a] | 0.03-0.3[h] | 112-88[i] | 1.37E+9 |
| Veerappan [19] | 180 | 12 | 1-4/14 | 23-47 @480 | 4-7 | 0.28-16[d] | 0.2[j] | 161-141[i] | 2.78E+9 |
| Veerappan [21] | 180 | 12 | 1-12/25 | 18-47 @520 | 2-8 | 0.2-6[d] | 7.2[k] | 139-101[i] | 5.88E+9 |
| Xu [22] | 150 | 10 | 2-5/19 | 24-32 @450 | 2-3.5 | 0.1-1 | 1-13[l] | 42[m] | 1.33E+11 |
| Lee [20] | 140(SOI) | 12 | 0.5-3/11 | 12-25 @500 | 2.5-7 | 0.9-260 | 1.7[n] | 65[o] | 1.17E+9 |
| Richardson [13] | 130 | 8 | 0.6-1.4/14 | 18-28 @500 | 3-5 | 0.24-0.6[a] | 0.02[p] | 200[q] | 9.04E+9 |
| Richardson [12] | 130 | 8 | 0.2-1.2/12-18 | 18-33 @450 | 2-5 | 0.4-0.8 | 0.02[r] | 237-184[s] | 4.01E+10 |
| Niclass [10] | 130 | 10 | 1-3.5/10 | 31-41 @450 | 3 | 120-1300[d] | N/A | 144[i] | N/A |
| Niclass [43] | 180 | 25 | 5/20.5 | 64.8 @610[ii] | 24 | 0.6 | 0.49[dd] | 190 | 1.83E+11 |
| Gersbach [11] | 130 | 4.3 | 1-2/9 | 18-30 @480 | 3.5-5 | 1.5-11.5 | <1[t] | 125[i] | 3.89E+9 |
| Charbon [15] | 65 | 8 | 0.05-0.4/9 | 2-5.5 @420 | 0.2-0.4 | 340-15.6k[a] | <1[u] | 235[i] | 3.71E+5 |
| Sanzaro(A) [24] | 160(BCD) | 10-80 | 3-9/36 | 31-58 @450 | 2.5-6.5 | 0.12-0.2[v] | 0.43-1.59[w] | 39-28[c] | 9.12E+11 |
| Sanzaro(B) [24] | 160(BCD) | 10-80 | 3-9/25 | 2-47 @450 | 2.5-6.5 | 0.1-0.18[v] | 0.02-0.14[w] | 36-28[c] | 7.9E+11 |
| Sanzaro(C) [24] | 160(BCD) | 10-80 | 3-9/26 | 55-71 @490 | 6-9 | 0.13-0.19[v] | 0.41-1.26[w] | 41-28[c] | 1.15E+12 |
| Pellegrini [25] | 40 | 18.36 | 1/15.5 | 45 @460[+] | 5 | N/A[†] | 0.1 | 170[*] | N/A |
| Nolet [5] | 65 | 20 | 1.75/9.9 | 8 @470 | N/A | 2.8k | <10 | 7.8[♯] | N/A |
| Webster [14] | 90 | 6.4 | 14.9/2.4 | 44 @700 | 22 | 8.1k | 0.375 | 84 | N/A |
| **This Work** | **180** | **25-100** | **1-11/22** | **25-55@480**[2] | **3-8.4**[x] | **0.06-0.23**[y] | **~0.12-3**[z] | **12.1**[1] | **2.78E+13** |

[a] At 20°C. [b] 200$\mu m$-diameter, at 25°C, 80 ns dead time, $V_{EX}$=5V. [c] 820 nm wavelength. [d] At 25°C. [dd] 24 ns dead time. [e] 30 $\mu$m-diameter, at 25°C, 40 ns dead time, $V_{EX}$=5 V, integrated AQC. [f] A time resolution of 28-37 ps FWHM and a diffusion tail of 160-340 ps were demonstrated in Ref. [45] using the substrate bias as a trade-off parameter between jitter and diffusion tail. [g] PDE=10-13% at 800 nm. [h] 300 ns dead time, $V_{EX}$=2-10 V. [i] 637 nm wavelength. [ii] Substrate not isolated SPAD. [j] 300 ns dead time, $V_{EX}$=4V. [k] 300 ns dead time, $V_{EX}$=11 V. [l] 50 ns dead time, $V_{EX}$=1.5-5 V. [m] 831 nm wavelength. [n] 200 ns dead time, $V_{EX}$=2V. [o] 405 nm wavelength. [p] 200 ns dead time, $V_{EX}$=2V. [q] 815 nm wavelength. [r] 50 ns dead time. [s] 470 nmwavelength. [t] 180 ns dead time. [u] 5$\mu s$ dead time. [v] At 300 K. [w] 30$\mu m$-diameter, at 300 K, 50 ns dead time. [x] Measured between 1V and 6V excess bias at 25°C. [y] 25$\mu m$-diameter at 20°C measured at 1 V and 6 V excess bias. [z] For a dead time of 3 ns on the 25 $\mu m$-diameter and 100 $\mu m$-diameter SPADs at 25°C and 6 V excess bias. [*] 1 V excess bias, room temperature and 850nm laser. [+] Using microlenses. [†] About 100 cps at room temperature at 1V excess bias. [♯] 410 nm laser. [1] 25$\mu m$-diameter at 20°C with an excess bias of 6V. [2] value taken at 1 V and 6 V excess bias.

Recently, a number of SPAD imagers has also been used in quantum distillation [48], quantum LiDAR [49,50], and quantum plenoptic cameras [51], where pairs of entangled photons generated through spontaneous parametric downconversion (SPDC) are employed extract appropriate information from scenes suffering from extensive background illumination and challenging interpretation [52]. The figure below shows a micrograph of the first megapixel SPAD image sensor, MegaX [32].

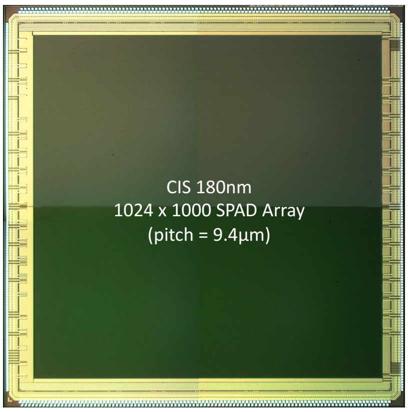


K. Morimoto et al., Optica 2020

**Figure 198-3. The MegaX chip.**

This sensor was employed in several classical applications, like the light-in-flight experiments, LiDAR imaging, and widefield FLIM, and quantum imaging applications, like quantum distillation and quantum LiDAR. Quantum imaging, though, requires not only single-photon detection, but also dedicated architectures enabling to use photogenerated pulses *in situ* or at least not to degrade the timing resolution of the detection. The principles and architectures recently emerged to implement quantum and classical imaging using SPAD sensors and the challenges of such implementations at system level focus on the promise of better resolution, PDE, DCR, and especially pixel count [52,53,54]. In addition, with the introduction of larger formats in SPAD imagers, several applications introduced earlier in the literature have been improved. This is so especially in the presence of massive radiation and background illumination. Examples are non-line-of-sight imaging [54,55,56] and diffuse imaging [57,58]. At the same time, new imaging modalities, such as quanta burst photography (QBP) [59], quantum state tomography, and quantum holography are emerging. Researchers involved in these activities request multi-megapixel SPAD cameras, along with RGB and non-Bayer color filters for low-light illumination applications, as well as multi-spectral and hyper-spectral filter patterns. Similarly, reconfigurable SPAD sensors are sought to achieve solutions capable of adapting to various conditions of illumination and dynamic of the scene. One such example has recently been proposed in [60].

In conclusion, the field of single-photon imaging has found its application in a wide variety of imaging modalities, which require an increasingly rich set of specifications. Emerging computational imaging and quantum imaging are increasingly demanding larger formats and more computation *in situ*. This trend is opening the use of natively digital photodetectors, such as SPADs, to localized processing and artificial intelligence, which is currently under development and will be facilitated by the economy of scale of CMOS applied to SPADs, enabling lower power, higher functionality, and scalable designs. This is a clear trend for the future.

## REFERENCES

[1] S. Cova, M. Ghioni, A. Lacaita, C. Samori, and F. Zappa, "Avalanche photodiodes and quenching circuits for single-photon detection," Applied Optics, **35**(12), 1956–1976 (1996).

[2] F. Ceccarelli, G. Acconcia, A. Gulinatti, M. Ghioni, I. Rech, and R. Osellame, "Recent advances and future perspectives of single photon avalanche diodes for quantum photonics applications," Advanced Quantum Technologies, 2000102 (2020).

[3] S. Cova, A. Lacaita, M. Ghioni, G. Ripamonti, and T. Louis, "20-ps timing resolution with single-photon avalanche diodes," Review of Scientific Instruments, **60**(6), 1104–1110 (1989).

[4] A. Spinelli, M. A. Ghioni, S. D. Cova, and L. M. Davis, "Avalanche detector with ultraclean response for time-resolved photon counting," IEEE Journal of Quantum Electronics, **34**(5), 817–821 (1998).

[5] F. Nolet, S. Parent, N. Roy, M.-O. Mercier, S. Charlebois, R. Fontaine, and J.-F. Pratte, "Quenching circuit and SPAD integrated in CMOS 65nm with 7.8 ps FWHM single photon timing resolution," Instruments, **2**(19), (2018).

[6] M. Ghioni, S. Cova, A. Lacaita, and G. Ripamonti, "New silicon epitaxial avalanche diode for single-photon timing at room temperature," Electronics Letters, **24**(24), 1476–1477 (1988).

[7] M. Ghioni, A. Gulinatti, I. Rech, F. Zappa, and S. Cova, "Progress in silicon single-photon avalanche diodes," IEEE Journal of Selected Topics in Quantum Electronics, **13**(4), 852–862 (2007).

[8] A. Gulinatti, I. Rech, F. Panzeri, C. Cammi, P. Maccagnani, M. Ghioni, and S. Cova, "New silicon SPAD technology for enhanced red sensitivity, high-resolution timing and system integration," Journal of Modern Optics, **59**(17), 1489–1499 (2012).

[9] A. Rochas, M. Gani, B. Furrer, P. Besse, R. Popovic, G. Ribordy, and N. Gisin, "Single photon detector fabricated in a complementary metal–oxide–semiconductor high-voltage technology," Review of Scientific Instruments, **74**(7), 3263–3270 (2003).

[10] C. Niclass, M. Gersbach, R. Henderson, L. Grant, and E. Charbon, "A single photon avalanche diode implemented in 130-nm CMOS technology," IEEE Journal of Selected Topics in Quantum Electronics, **13**(4), 863–869 (2007).

[11] M. Gersbach, C. Niclass, E. Charbon, J. Richardson, R. Henderson, and L. Grant, "A single photon detector implemented in a 130nm CMOS imaging process," in European Solid-State Device Research Conference (ESSCIRC), 270–273 (2008).

[12] J. A. Richardson, E. A. G. Webster, L. A. Grant, and R. K. Henderson, "Scaleable single-photon avalanche diode structures in nanometer CMOS technology," IEEE Trans. Electron Devices, **58**(7), 2028–2035 (2011).

[13] J. A. Richardson, L. A. Grant, and R. K. Henderson, "Low dark count single-photon avalanche diode structure compatible with standard nanometer scale CMOS technology," IEEE Photonics Technology Letters, **21**(14), 1020–1022 (2009).

[14] E. A. G. Webster, J. A. Richardson, L. A. Grant, D. Renshaw, and R. K. Henderson, "A single-photon avalanche diode in 90-nm CMOS imaging technology with 44% photon detection efficiency at 690 nm," IEEE Electron Device Letters, **33**(5), 694–696 (2012).

[15] E. Charbon, H. Yoon, and Y. Maruyama, "A Geiger mode APD fabricated in standard 65nm CMOS technology," in 2013 IEEE International Electron Devices Meeting, 27.5.1–27.5.4 (2013).

[16] F. Villa, D. Bronzi, Y. Zou, C. Scarcella, G. Boso, S. Tisa, A. Tosi, F. Zappa, D. Durini, S. Weyers, U. Paschen, and W. Brockherde, "CMOS SPADs with up to 500μm diameter and 55% detection efficiency at 420nm," Journal of Modern Optics, **61**(2), 102–115 (2014).

[17] T. Leitner, A. Feiningstein, R. Turchetta, R. Coath, S. Chick, G. Visokolov, V. Savuskan, M. Javitt, L. Gal, I. Brouk, S. Bar-Lev, and Y. Nemirovsky, "Measurements and simulations of low dark count rate single photon avalanche diode device in a low voltage 180-nm CMOS image sensor technology," IEEE Transactions on Electron Devices, **60**(6), 1982–1988 (2013).

[18] C. Veerappan and E. Charbon, “A substrate isolated CMOS SPAD enabling wide spectral response and low electrical crosstalk,” IEEE Journal of Selected Topics in Quantum Electronics, **20**(6), 299–305 (2014).

[19] C. Veerappan and E. Charbon, “CMOS SPAD based on photo-carrier diffusion achieving PDP >40% from 440 to 580 nm at 4 V excess bias,” IEEE Photonics Technology Letters, **27**, 2445–2448 (2015).

[20] M.-J. Lee, P. Sun, and E. Charbon, “A first single-photon avalanche diode fabricated in standard SOI CMOS technology with a full characterization of the device,” Optics Express, **23**(10), 13 200–13 209, (2015).

[21] C. Veerappan and E. Charbon, “A low dark count p-i-n diode based SPAD in CMOS technology,” IEEE Transactions on Electron Devices, **63**, 65–71 (2016).

[22] H. Xu, L. Pancheri, G.-F. D. Betta, and D. Stoppa, “Design and characterization of a p+/n-well SPAD array in 150nm CMOS process,” Optics Express, **25**(11), 12 765–12 778, (2017).

[23] C. Veerappan, “Single-photon avalanche diodes for cancer diagnosis,” Ph.D. dissertation, Delft University of Technology, Delft, Netherlands (2016).

[24] M. Sanzaro, P. Gattari, F. Villa, A. Tosi, G. Croce, and F. Zappa, “Single-photon avalanche diodes in a 0.16 μm BCD technology with sharp timing response and red-enhanced sensitivity,” IEEE Journal of Selected Topics in Quantum Electronics, **24**(2), 3801209 (2017).

[25] S. Pellegrini, B. Rae, A. Pingault, D. Golanski, S. Jouan, C. Lapeyre, and B. Mamdy, “Industrialised SPAD in 40 nm technology,” in IEEE International Electron Devices Meeting (IEDM), 16.5.1–16.5.4 (2017).

[26] J. Mata Pavia, M. Scandini, S.A. Lindner, M. Wolf, E. Charbon, “A 1×400 Backside-Illuminated SPAD Sensor with 49.7ps Resolution, 30 pJ/Sample TDCs Fabricated in 3D CMOS Technology for Near-Infrared Optical Tomography”, Journal of Solid-State Circuits, **50**(10), 2406-2418 (2015).

[27] C. Bruschini, H. Homulle, I. M. Antolovic, S. Burri, and E. Charbon, “Single-photon avalanche diode imagers in biophotonics: review and outlook,” Light: Science & Applications, **8**(1), 87, (2019).

[28] X. Michalet, A. Ingargiola, R. A. Colyer, G. Scalia, S. Weiss, P. Maccagnani, A. Gulinatti, I. Rech, and M. Ghioni, “Silicon photon counting avalanche diodes for single-molecule fluorescence spectroscopy,” IEEE Journal of Selected Topics in Quantum Electronics, **20**(6), 248–267 (2014).

[29] G. Buller and A. Wallace, “Ranging and three-dimensional imaging using time-correlated single-photon counting and point-by-point acquisition,” IEEE Journal of Selected Topics in Quantum Electronics, **13**(4), 1006–1015 (2007).

[30] H. Takesue, E. Diamanti, C. Langrock, M. Fejer, and Y. Yamamoto, “10-GHz clock differential phase shift quantum key distribution experiment,” Optics Express, **14**(20), 9522–9530 (2006).

[31] A. C. Ulku, C. Bruschini, I. M. Antolovi´c, Y. Kuo, R. Ankri, S. Weiss, X. Michalet, and E. Charbon, “A 512 × 512 SPAD image sensor with integrated gating for widefield flim,” IEEE Journal of Selected Topics in Quantum Electronics, **25**(1), 1–12, (2019).

[32] K. Morimoto, A. Ardelean, M.-L. Wu, A. C. Ulku, I. M. Antolovic, C. Bruschini, and E. Charbon, “Megapixel time-gated SPAD image sensor for 2D and 3D imaging applications,” Optica, **7**(4), 346–354 (2020).

[33] S. Lindner, S. Pellegrini, Y. Henrion, B. Rae, M. Wolf, and E. Charbon, “A high-PDE, backside-illuminated SPAD in 65/40-nm 3D IC CMOS pixel with cascoded passive quenching and active recharge,” IEEE Electron Device Letters, **38**(11), 1547–1550 (2017).

[34] I. M. Antolovic, C. Bruschini, and E. Charbon, “Dynamic range extension for photon counting arrays,” Optics Express, **26**(17), 22 234–22 248 (2018).

[35] P. Mroszczyk and P. Dudek, “Tunable CMOS delay gate with improved matching properties,” IEEE Transactions on Circuits and Systems I: Regular Papers, **61**(9), 2586–2595 (2014).

[36] B. Korzh, T. Lunghi, K. Kuzmenko, G. Boso, and H. Zbinden, “Afterpulsing studies of low-noise InGaAs/InP single-photon negative feedback avalanche diodes,” Journal of Modern Optics, **62**(14), 1151–1157 (2015).

[37] Z. Cheng, X. Zheng, D. Palubiak, M. J. Deen, and H. Peng, “A comprehensive and accurate analytical SPAD model for circuit simulation,” IEEE Transactions on Electron Devices, **63**(5), 1940–1948 (2016).

[38] M. Anti, A. Tosi, F. Acerbi, and F. Zappa, “Modeling of afterpulsing in single-photon avalanche diodes,” in Physics and Simulation of Optoelectronic Devices XIX, B. Witzigmann, F. Henneberger, Y. Arakawa, and A. Freundlich, Eds., vol. 7933, International Society for Optics and Photonics. SPIE, 2011, 371 – 378 (2011).

[39] S. Cova, A. Lacaita, and G. Ripamonti, “Trapping phenomena in avalanche photodiodes on nanosecond scale,” IEEE Electron Device Lett., **12**(12), 685–687 (1991).

[40] G. Zappalà, F. Acerbi, A. Ferri, A. Gola, G. Paternoster, N. Zorzi, and C. Piemonte, “Set-up and methods for SiPM photo-detection efficiency measurements,” Journal of Instrumentation, **11**(08), P08014 (2016).

[41] S. K. Yang, J. Lee, S.-W. Kim, H.-Y. Lee, J.-A. Jeon, I. H. Park, J.-R. Yoon, and Y.-S. Baek, “Precision measurement of the photon detection efficiency of silicon photomultipliers using two integrating spheres,” Optics Express, **22**(1), 716–726 (2014).

[42] W.-Y. Ha, E. Park, D. Eom, H.-S. Park, F. Gramuglia, P. Keshavarzian, E. Kizilkan, C. Bruschini, D. Chong, S.S. Tan, M. Tng, E. Quek, E. Charbon, W.-Y. Choi, M.-J. Lee, “SPAD Developed in 55 nm Bipolar-CMOS-DMOS Technology Achieving Near 90% Peak PDP,” IEEE Journal of Selected Topics in Quantum Electronics, (2023).

[43] C. Niclass, H. Matsubara, M. Soga, M. Ohta, M. Ogawa, and T. Yamashita, “A NIR-sensitivity-enhanced single-photon avalanche diode in 0.18μm CMOS,” in Proceedings of the International Image Sensor Workshop, Vaals, The Netherlands, 8–11

(2015).

[44] D. Bronzi, F. Villa, S. Tisa, A. Tosi, and F. Zappa, "SPAD figures of merit for photon-counting, photon-timing, and imaging applications: A review," IEEE Sensors Journal, **16**(1), 3–12 (2016).

[45] M. Buttafava, G. Boso, A. Ruggeri, A. Dalla Mora, and A. Tosi, "Time-gated single-photon detection module with 110 ps transition time and up to 80 MHz repetition rate," Review of Scientific Instruments, **85**(8), 083114 (2014).

[46] F. Gramuglia, M.-L. Wu, C. Bruschini, M.J. Lee, E. Charbon, "A Low-noise CMOS SPAD Pixel with 12.1 ps SPTR and 3 ns Dead Time," IEEE Journal of selected Topics in Quantum Electronics, **28**(2), 1-9 (2021).

[47] F. Gramuglia, E. Ripiccini, C.A. Fenoglio, M.L. Wu, L. Paolozzi, C. Bruschini, E. Charbon, "Direct MIP detection with sub-10 ps timing resolution Geiger-Mode APDs", Nuclear Instruments and Methods in Physics Research Section A: Accelerators (NIM-A), **1047**, 167813 (2023).

[48] H. Defienne, M. Reichert, J. W. Fleischer, and D. Faccio, "Quantum image distillation," Science Advances **5**(10), eaax0307 (2019).

[49]. J. Zhao et al., "Light detection and ranging with entangled photons", Optics Express **30**(3), 3675-3683 (2022).

[50] S. Frick, A. McMillan, and J. Rarity, "Quantum rangefinding," Optics Express **28**(25), 37118–37128 (2020).

[51] C Abbattista et al., "Towards quantum 3D imaging devices", Applied Sciences 11(14), 6414 (2021).

[52] P. Bruza et al., "Single-photon avalanche diode imaging sensor for subsurface fluorescence LiDAR", Optica **8**(8), 1126-1127 (2021).

[53] H. Defienne, J. Zhao, E. Charbon, and D. Faccio, "Full-field quantum imaging with a single-photon avalanche diode camera," Phys. Rev. A **103**(4), 042608 (2021).

[54] A. Velten, et al., "Recovering three-dimensional shape around a corner using ultrafast time-of-flight imaging," Nature Communications **3**(1), 745 (2012).

[55] G. Gariepy, F. Tonolini, R. Henderson, J. Leach, and D. Faccio, "Detection and tracking of moving objects hidden from view", Nature Photonics **10**(1), 23–26 (2016).

[56] M. O'Toole, D. B. Lindell, and G.Wetzstein, "Confocal non-line-of-sight imaging based on the light-cone transform", Nature **555**(7696), 338–341 (2018).

[57] A. Lyons, F. Tonolini, A. Boccolini, A. Repetti, R. Henderson, Y.Wiaux, and D. Faccio, "Computational time-of-flight diffuse optical tomography," Nature Photonics **13**(8), 575–579 (2019).

[58] T. Gregory, P.-A. Moreau, E. Toninelli, and M. J. Padgett, "Imaging through noise with quantum illumination," Science Advances **6**(6), eaay2652 (2020).

[59] S. Ma, S. Gupta, A.C. Ulku, C. Bruschini, E. Charbon, M. Gupta, "Quanta burst photography," ACM Transactions on Graphics (TOG), **39**(4), 79:1-79:16 (2020).

[60] V. Sundar, A. Ardelean, T. Swedish, C. Bruschini, E. Charbon, M. Gupta, "SoDaCam: Software-defined Cameras via Single-Photon Imaging," Preprint arXiv:2309.00066 (2023).